AGU PUBLICATIONS

Global Biogeochemical Cycles

RESEARCH ARTICLE
10.1002/2016GB005527

Key Points:
- Annual air-sea CO_2 flux (ocean carbon uptake) is greatest in the western North Pacific and decreases eastward across the basin
- Annually, biological carbon export fully offsets ocean carbon uptake from the atmosphere in the eastern but not the western North Pacific
- The influence of biological carbon export on air-sea CO_2 flux depends on the seasonal timing of export and ventilation

Supporting Information:
- Supporting Information S1

Correspondence to:
H. I. Palevsky,
hpalevsky@whoi.edu

Citation:
Palevsky, H. I., and P. D. Quay (2017), Influence of biological carbon export on ocean carbon uptake over the annual cycle across the North Pacific Ocean, *Global Biogeochem. Cycles*, *31*, 81–95, doi:10.1002/2016GB005527.

Received 12 SEP 2016
Accepted 2 JAN 2017
Accepted article online 5 JAN 2017
Published online 21 JAN 2017

©2017. American Geophysical Union. All Rights Reserved.

Influence of biological carbon export on ocean carbon uptake over the annual cycle across the North Pacific Ocean

Hilary I. Palevsky[1,2] and Paul D. Quay[1]

[1]School of Oceanography, University of Washington, Seattle, Washington, USA, [2]Now at Marine Chemistry and Geochemistry Department, Woods Hole Oceanographic Institution, Woods Hole, Massachusetts, USA

Abstract We evaluate the influences of biological carbon export, physical circulation, and temperature-driven solubility changes on air-sea CO_2 flux across the North Pacific basin (35°N–50°N, 142°E–125°W) throughout the full annual cycle by constructing mixed layer budgets for dissolved inorganic carbon (DIC) and pCO_2, determined on 15 container ship transects between Hong Kong and Long Beach, CA, from 2008 to 2012. Annual air-sea CO_2 flux is greatest in the western North Pacific and decreases eastward across the basin (2.7 ± 0.9 mol C m^{-2} yr^{-1} west of 170°E, as compared to 2.1 ± 0.3 mol C m^{-2} yr^{-1} east of 160°W). East of 160°W, DIC removal by annual net community production (NCP) more than fully offsets the DIC increase due to air-sea CO_2 flux. However, in the region west of 170°E influenced by deep winter mixing, annual NCP only offsets ~20% of the DIC increase due to air-sea CO_2 flux, requiring significant DIC removal by geostrophic advection. Temperature-driven solubility changes have no net influence on pCO_2 and account for <25% of annual CO_2 uptake. The seasonal timing of NCP strongly affects its influence on air-sea CO_2 flux. Biological carbon export from the mixed layer has a stronger influence on pCO_2 in summer when mixed layers are shallow, but changes in pCO_2 have a stronger influence on air-sea CO_2 flux in winter when high wind speeds drive more vigorous gas exchange. Thus, it is necessary to determine the seasonal timing as well as the annual magnitude of NCP to determine its influence on ocean carbon uptake.

1. Introduction

The ocean currently absorbs 26% of all anthropogenic carbon emissions [*Le Quéré et al*., 2015], slowing global climate change by reducing carbon accumulation in the atmosphere and modifying marine chemistry by redistributing this carbon into the ocean. Much attention has thus been focused on understanding the mechanisms controlling the rates and spatial patterns of ocean carbon uptake [e.g., *Takahashi et al*., 2002, 2009; *Wanninkhof et al*., 2013; *Landschützer et al*., 2014]. There are three main mechanisms that drive exchange of CO_2 between the ocean and the atmosphere: chemical effects due to temperature- and salinity-dependent variation in the solubility of CO_2 in seawater; biological effects due to fixation and export of organic carbon and biogenic $CaCO_3$ from the surface ocean; and physical effects due to advection and mixing, which can sequester carbon from the atmosphere by transporting CO_2 absorbed at the surface into the deep ocean. Understanding the relative roles of these chemical, physical, and biological processes is necessary to improve our ability to mechanistically predict how the ocean carbon sink will respond to and exert a feedback influence on increasing atmospheric CO_2 concentrations and climate changes projected for the 21st century [e.g., *Roy et al*., 2011; *Ciais et al*., 2013; *Hauck et al*., 2015].

The North Pacific is a major sink for atmospheric CO_2, featuring a band of strong CO_2 uptake at the transition zone between the subarctic gyre to the north and the subtropical gyre to the south [*Takahashi et al*., 2009] (Figure 1). Previous studies have used a variety of observational and analytical approaches to quantify the contributions of temperature-driven solubility effects, physical circulation, and biological carbon export to the North Pacific carbon sink. *Takahashi et al*. [2002] presented a simple approach to separate temperature and non-temperature effects on observed seasonal cycles of surface ocean partial pressure of CO_2 (pCO_2). Applying this approach to both observations and global biogeochemical model output reveals opposite-phase temperature-driven and non-temperature-driven seasonal cycles. Temperature effects dominate in the subtropical and much of the eastern subarctic North Pacific and non-temperature effects of biological pCO_2 drawdown and physical pCO_2 supply dominate in the high-latitude and western subarctic North Pacific, with a region of more complex balance at the interface between these two regimes [*Takahashi*

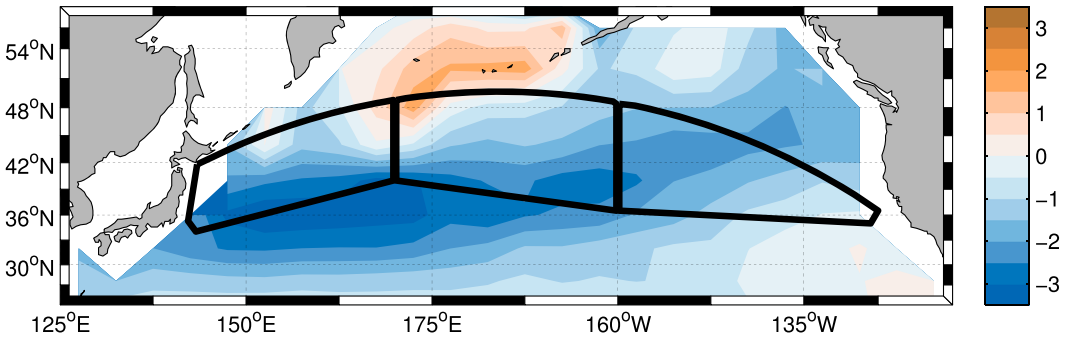

Figure 1. Locations of the three container ship sampling regions are outlined in black (from west to east, the Kuroshio, West, and East) and shown over a map of climatological mean annual air-sea CO_2 flux (mol C m^{-2} yr^{-1}) normalized to the year 2000 (data from *Takahashi et al*. [2009]).

et al., 2002; *Chierici et al*., 2006; *McKinley et al*., 2006]. Recent work explicitly separating non-temperature effects into physical and biological components concluded that despite their large effect on the seasonal cycle, temperature-driven changes in solubility drive only a small portion of annual CO_2 uptake, with geostrophic advection joining biological carbon export as the dominant drivers of strong CO_2 uptake and setting the location of the strong transition zone CO_2 sink [*Ayers and Lozier*, 2012].

Opportunities to evaluate seasonal and annual effects on the ocean carbon sink over a basin-wide scale using direct measurements of both carbonate chemistry and biological carbon export rates are rare. Previous observation-based basin-scale analyses have combined carbonate chemistry measurements from repeat ship of opportunity transects with estimates of biological carbon export based on seasonal nitrate drawdown [*Wong et al*., 2002; *Chierici et al*., 2006] or used climatological carbonate chemistry data and estimated biological carbon export from satellite-based primary production and export efficiency algorithms [*Ayers and Lozier*, 2012]. These approaches are limited, however, by discrepancies between satellite- and geochemical observation-based estimates of seasonal biological carbon export [*Palevsky et al*., 2016a] and the inability of either satellite-based estimates or measurements of nitrate drawdown to account for the fraction of seasonally exported organic matter that is subsequently ventilated back to the atmosphere as CO_2 during deep winter mixing, which has a strong influence on annual biological carbon export in the western North Pacific [*Palevsky et al*., 2016b].

In this study, we use measurements of the complete carbonate chemistry system on 15 basin-wide transects across the North Pacific on ships of opportunity to quantify the rate and the physical, chemical, and biological drivers of air-sea CO_2 flux across the entire North Pacific throughout the full annual cycle. Seasonal and annual rates of biological carbon export (defined as net community production, or NCP) have recently been determined based on measurements of dissolved O_2/Ar gas ratios measured on the same set of ship of opportunity transects [*Palevsky et al*., 2016b]. The combination of measured carbonate chemistry with O_2/Ar-based estimates of NCP on a basin-wide scale throughout the full annual cycle provides a unique opportunity to resolve the role of biological carbon export in driving the North Pacific Ocean carbon sink.

2. Regional Setting

Carbonate chemistry data presented here are interpreted in the context of three broad regions across the North Pacific, as defined by *Palevsky et al*. [2016b]: the Kuroshio, west of 170°E, partially influenced by the Kuroshio, Oyashio, and Kuroshio Extension currents; the Western region, between 170°E and 160°W; and the Eastern region, east of 160°W (Figure 1). These regions include portions of both the physical transition zone between the subarctic and subtropics between 32°N and 42°N [*Roden*, 1991] and the high-nutrient low-chlorophyll subarctic gyre to the north [*Harrison et al*., 2004]. Superimposed on these physical gradients, the transition zone chlorophyll front migrates seasonally across the region, with its southernmost extent in February largely south of our three study regions, while its northernmost extent in August lies at ~40°N, in the middle of our regions [*Polovina et al*., 2001; *Ayers and Lozier*, 2010].

Our regional division scheme focuses on analysis of east-west basin-wide trends. The western basin is more dynamically complex, with portions of this region influenced both by strong eastward geostrophic transport

by the Kuroshio Extension and by deep winter mixing (<200 m) [*Jayne et al*., 2009; *Ohno et al*., 2009]. The eastern side of the basin experiences weaker geostrophic transport and has a strong permanent halocline at ~120 m that limits the extent of winter mixing [*Harrison et al*., 1999]. Primary production rates, as determined by analysis of triple oxygen isotope samples collected along the same container ship transects described in this study, are greatest in the Kuroshio and decrease eastward across the basin, likely due both to greater nutrient supply from deeper winter mixing and greater aeolian dust (iron) supply in the west [*Palevsky et al*., 2016b]. Analysis of dissolved O_2/Ar gas ratios measured on the same samples indicate that spring through fall NCP rates are also greatest in the Kuroshio and decrease eastward across the basin. However, wintertime O_2/Ar measurements indicate that much of the seasonally exported organic material is subsequently remineralized and is ventilated back to the atmosphere during winter mixing. Winter mixed layer depths and thus the fraction of seasonally exported material that is ventilated to the atmosphere as CO_2 increase westward across the basin, such that annual NCP rates integrated to the winter ventilation depth (defined as the deepest depth ventilated to the atmosphere during winter mixing) are greatest in the east and decrease westward across the basin, yielding the opposite trend to productive season export [*Palevsky et al*., 2016b].

3. Methods

3.1. Sample Collection and Measurement

Samples for carbonate chemistry analysis were collected from shipboard seawater intake (10 m depth) on 15 basin-wide transects of the North Pacific between Hong Kong and Long Beach, California, on board the M/V *OOCL Tianjin* and the M/V *OOCL Tokyo* between October 2008 and December 2012 (Figures 1 and S1 in the supporting information). Sea surface temperature (SST) and salinity (*S*) at the time of sample collection were determined using a Sea-Bird Electronics SBE45 thermosalinograph installed in the ship's seawater intake. Carbonate chemistry sampling locations largely correspond with locations of sample collection for analysis of dissolved O_2/Ar ratios as a tracer of net community production (NCP), as presented by *Palevsky et al*. [2016b], allowing us to interpret carbonate chemistry data alongside NCP results.

Samples for dissolved inorganic carbon (DIC) analysis were collected on all cruises into 250 mL bottles with greased ground glass stoppers and poisoned with 100 μL of saturated mercuric chloride solution. DIC concentrations were determined in the laboratory through a combination of manometric measurements [*Quay and Stutsman*, 2003] ($n = 320$) and measurements with an Apollo SciTech AS-C3 IR-based DIC analyzer ($n = 138$). Certified reference materials (Andrew Dickson, UCSD) were used for calibration and determination of sample-specific measurement error for all DIC measurements using the AS-C3 analyzer, with mean uncertainty of $\pm 4\ \mu mol\ kg^{-1}$. Comparison of duplicate samples analyzed both manometrically and with the AS-C3 analyzer ($n = 111$) agree to within $1 \pm 9\ \mu mol\ kg^{-1}$ and indicate uncertainty of $\pm 8\ \mu mol\ kg^{-1}$ in the manometric measurements.

A second carbonate chemistry parameter was determined for all locations with DIC measurements. For transects from 2008 to 2010, pCO_2 was measured using an automated underway IR-detection-based system, which determines seawater pCO_2 to ± 2 μatm [*Feely et al*., 1998; *Pierrot et al*., 2009; data available online at http://www.pmel.noaa.gov/co2/story/Long+Beach+to+Hong+Kong]. Measurements from this system were made continuously along the cruise tracks and were extracted at locations corresponding to DIC sample collection. For transects in 2011–2012, the underway pCO_2 system was not used and instead discrete samples were collected to determine total alkalinity (TA) at DIC sampling locations, following the same collection procedures as for DIC. TA samples were measured using an automated, open-cell potentiometric titration system [*Dickson et al*., 2007] (SOP 3b), with sample-specific measurement error quantified based on certified reference materials (Andrew Dickson, UCSD) measured with each sample batch (mean uncertainty of $\pm 2\ \mu eq\ kg^{-1}$). For a small fraction of DIC sampling locations ($n = 51$), neither underway pCO_2 nor discrete measurements of TA were available due to issues with the underway pCO_2 system or lost samples during TA analysis. For these sampling locations, TA was determined using regional TA-salinity relationships determined from the measured TA samples (Figure S2).

For all locations, the combination of DIC with either TA or pCO_2 fully constrains the carbonate chemistry system. The parameter not measured (either TA or pCO_2) was calculated for each sampling location using

the program CO2sys [*van Heuven et al.*, 2011] with the carbonate constants of *Mehrbach et al.* [1973] refit by *Dickson and Millero* [1987]. These constants are also used in all carbonate chemistry calculations throughout this work. Uncertainty in each calculated carbonate chemistry parameter was determined using a Monte Carlo approach, where 3000 calculations were made with CO2sys while allowing the two carbonate chemistry input parameters to vary according to sample-specific measurement uncertainty. Mean uncertainty in TA calculated from DIC and pCO_2 is $\pm 9\,\mu eq\,kg^{-1}$ and mean uncertainty in pCO_2 calculated from DIC and TA is $\pm 16\,\mu atm$. Seasonal mean DIC, TA, and pCO_2 were calculated for each region, with methodological uncertainty (1σ) determined using a Monte Carlo 3000-simulation analysis where each individual sampling location value varied according to sample-specific measurement uncertainty.

The remainder of this paper focuses on processes influencing DIC and pCO_2. A corresponding budget showing processes influencing TA, which are less well constrained from this data set, is presented in the supporting information.

3.2. Processes Influencing DIC and pCO_2

Seasonal changes in observed DIC concentrations in the surface mixed layer ($mmol\,m^{-3}\,d^{-1}$) are influenced by air-sea CO_2 flux (Gas), biological export of organic carbon (net community production, or NCP), biological production of calcium carbonate ($CaCO_3$), and physical addition or removal of DIC due to advection and mixing (Physics).

$$\frac{\partial \mathrm{DIC}}{\partial t} = \left.\frac{\partial \mathrm{DIC}}{\partial t}\right|_{\mathrm{Gas}} + \left.\frac{\partial \mathrm{DIC}}{\partial t}\right|_{\mathrm{NCP}} + \left.\frac{\partial \mathrm{DIC}}{\partial t}\right|_{\mathrm{CaCO_3}} + \left.\frac{\partial \mathrm{DIC}}{\partial t}\right|_{\mathrm{Physics}} \quad (1)$$

Each term in equation (1) is calculated seasonally for each of the three regions shown in Figure 1. Seasonal fluxes for the Gas, NCP, and $CaCO_3$ terms ($mmol\,m^{-2}\,d^{-1}$; details of flux estimation methods for each term given below) are converted to influences on the seasonal DIC concentration ($\mu mol\,kg^{-1}\,d^{-1}$) by multiplying by the regional mean $\frac{\rho}{\mathrm{MLD}}$ in each season, where ρ is the temperature- and salinity-dependent seawater density and MLD is the mixed layer depth, as determined by $0.125\,kg\,m^{-3}$ density increase from the surface [*Monterey and Levitus*, 1997] in World Ocean Atlas 2013 (WOA, https://www.nodc.noaa.gov/OC5/woa13) gridded temperature and salinity fields. Uncertainty in MLD estimates is calculated as the standard error $\left(\frac{2\sigma}{\sqrt{n}}\right)$ of the mean for each season in each region. The physical influence of advection and mixing is calculated as the residual based on estimates of all other terms in equation (1).

Seasonal changes in observed pCO_2 in the surface mixed layer are influenced by all factors that influence DIC, as well as effects of temperature and salinity on the solubility of CO_2.

$$\frac{\partial pCO_2}{\partial t} = \left.\frac{\partial pCO_2}{\partial t}\right|_{\mathrm{Temp}} + \left.\frac{\partial pCO_2}{\partial t}\right|_{\mathrm{Sal}} + \left.\frac{\partial pCO_2}{\partial t}\right|_{\mathrm{Gas}} + \left.\frac{\partial pCO_2}{\partial t}\right|_{\mathrm{NCP}} + \left.\frac{\partial pCO_2}{\partial t}\right|_{\mathrm{CaCO_3}} + \left.\frac{\partial pCO_2}{\partial t}\right|_{\mathrm{Physics}} \quad (2)$$

The individual right-hand side (RHS) terms can each be calculated following equations (3)–(7):

$$\left.\frac{\partial pCO_2}{\partial t}\right|_{\mathrm{Temp}} = \left(\frac{\partial \mathrm{SST}}{\partial \mathrm{t}}\right) \times pCO_2\left(0.0423\ ^{\circ}C^{-1}\right) \quad (3)$$

$$\left.\frac{\partial pCO_2}{\partial t}\right|_{\mathrm{Sal}} = \left(\frac{\partial S}{\partial t}\right) \times \frac{pCO_2}{S}(1.6) \quad (4)$$

$$\left.\frac{\partial pCO_2}{\partial t}\right|_{\mathrm{Gas}} = \left(\left.\frac{\partial \mathrm{DIC}}{\partial t}\right|_{\mathrm{Gas}}\right)\left(\frac{\partial pCO_2}{\partial \mathrm{DIC}}\right) \quad (5)$$

$$\left.\frac{\partial pCO_2}{\partial t}\right|_{\mathrm{NCP}} = \left(\left.\frac{\partial \mathrm{DIC}}{\partial t}\right|_{\mathrm{NCP}}\right)\left[\left(\frac{\partial pCO_2}{\partial \mathrm{DIC}}\right) - \frac{17}{117}\left(\frac{\partial pCO_2}{\partial \mathrm{TA}}\right)\right] \quad (6)$$

$$\left.\frac{\partial pCO_2}{\partial t}\right|_{\mathrm{CaCO_3}} = \left(\left.\frac{\partial \mathrm{DIC}}{\partial t}\right|_{\mathrm{CaCO_3}}\right)\left[\left(\frac{\partial pCO_2}{\partial \mathrm{DIC}}\right) + 2\left(\frac{\partial pCO_2}{\partial \mathrm{TA}}\right)\right] \quad (7)$$

The temperature- and salinity-dependences of CO_2 in equations (3) and (4) are from *Takahashi et al.* [1993] and *Sarmiento and Gruber* [2006], respectively (note that the salinity dependency value accounts for effects

of freshwater balance as well as the direct salinity effect). The air-sea CO_2 flux (Gas), NCP, and $CaCO_3$ dependencies in equations (5)–(7) represent changes to DIC and TA concentrations in the surface mixed layer, which in turn affect pCO_2. The influence of TA changes on pCO_2 are given based on the known stoichiometric relationships between DIC and TA changes for each process, where gas exchange does not affect TA, NCP increases TA by 17 mol for each 117 mol of DIC fixed to organic carbon [*Anderson and Sarmiento*, 1994], and $CaCO_3$ production decreases TA by 2 mol for each mole $CaCO_3$ produced due to removal of the doubly charged CO_3^{2-} ion. Sensitivity of pCO_2 to DIC and TA changes in equations (5)–(7), based on the Revelle and Alkalinity factors, is given by equations (8) and (9), respectively:

$$\frac{\partial pCO_2}{\partial DIC} = \frac{\text{Revelle Factor} \times pCO_2}{DIC} \tag{8}$$

$$\frac{\partial pCO_2}{\partial TA} = \frac{\text{Alkalinity Factor} \times pCO_2}{TA} \tag{9}$$

The Revelle and Alkalinity factors are defined as $\frac{\Delta pCO_2/pCO_2}{\Delta C/C}$, where C is DIC or TA for the Revelle or Alkalinity factors, respectively. These values are calculated using CO2sys and perturbations of $\pm 1\ \mu mol\ kg^{-1}$ to measured DIC and TA [*van Heuven et al*., 2011]. Seasonal mean values for each region are calculated for each individual term in equations (3)–(9) from the compilation of all discrete sample measurements. The physical influence of advection and mixing is calculated as the residual based on estimates of all other terms in equation (2), the same approach used to calculate physical influences in the DIC budget.

3.2.1. Time Rate of Change

To determine the DIC and pCO_2 time rate of change tendencies in equations (1) and (2) as well as the SST and salinity time rate of change tendencies in equations (3) and (4), all surface mixed layer measurements for each region are compiled into a single composite year, with the seasonal cycle determined by fitting simple harmonic functions using a least squares approach. The derivatives of these harmonic fits for the day of the year corresponding to collection of each discrete sample are compiled and used to calculate the seasonal mean time rate of change tendency of mixed layer DIC, pCO_2, SST, and S in each season for each of the three regions. Methodological uncertainty in the time rate of change of DIC and pCO_2 is calculated following a Monte Carlo approach based on 3000 iterations computing harmonic fits to the composite annual data while allowing each individual sampling location value to vary according to sample-specific measurement uncertainty.

3.2.2. Air-Sea CO_2 Flux

The rate of air-sea CO_2 gas flux is calculated from the difference in pCO_2 between the atmosphere and the surface ocean as

$$\left.\frac{\partial DIC}{\partial t}\right|_{Gas} = k_{CO_2} \times K_0 \times \left(pCO_{2,atmos} - pCO_{2,ocean}\right) \times \rho \tag{10}$$

where k_{CO_2} ($m\ d^{-1}$) is the air-sea gas transfer velocity for CO_2, K_0 ($mol\ kg^{-1}\ \mu atm^{-1}$) is the temperature- and salinity-dependent solubility of CO_2 [*Weiss*, 1974], and ρ is the seawater density ($kg\ m^{-3}$). When atmospheric pCO_2 exceeds (is less than) surface ocean pCO_2, gas exchange causes the value of $\left.\frac{\partial DIC}{\partial t}\right|_{Gas}$ to be positive (negative). Air-sea CO_2 flux rates are calculated for each individual discrete sample and then compiled to calculate mean values in each season for each of the three regions.

The value of $pCO_{2,atmos}$ was determined for the time and location of each discrete sample measurement of $pCO_{2,ocean}$ using NOAA Earth Systems Research Laboratory CarbonTracker (CT2015; http://www.esrl.noaa.gov/gmd/ccgg/carbontracker) atmospheric CO_2 mole fraction data on a global $3° \times 2°$ grid, averaged daily over the lowest two atmospheric pressure levels, and converted to a partial pressure of CO_2 using NCEP/NCAR reanalysis daily average atmospheric surface pressure (http://www.esrl.noaa.gov/psd/data/gridded/data.ncep.reanalysis.html), with an estimated uncertainty of $\pm 2\ \mu atm$. Daily wind speed data from the NOAA National Climactic Data Center's multiple-satellite Blended Sea Winds product (https://www.ncdc.noaa.gov/oa/rsad/air-sea/seawinds.html) were used to calculate k_{CO_2} for the time and location of each discrete sample following the *Nightingale et al*. [2000] relationship between k_{CO_2} and wind speed and the *Reuer et al*. [2007] weighting scheme. Uncertainty in the air-sea gas exchange rate is estimated by assuming that the majority of uncertainty results from the parameterized relationship between gas exchange rate (k_{CO_2}) and wind speed and that the spread between the air-sea gas exchange rates calculated from the *Liss and Merlivat* [1986] and *Wanninkhof* [1992] equations represents 95% of the variability ($\pm 2\sigma$) in k_{CO_2} [*Palevsky*

et al., 2013], yielding a mean uncertainty in k_{CO_2} of ±14% over all discrete sample locations in the data set. Total methodological uncertainty in seasonal and annual mean air-sea CO_2 flux in each region is determined with a Monte Carlo analysis including measurement uncertainty in atmospheric pCO_2, sample-specific uncertainty in seawater pCO_2, and uncertainty from estimation of the air-sea gas transfer rate.

3.2.3. Net Community Production and $CaCO_3$ Production

Biological processes influence DIC and pCO_2 through export of biologically fixed organic carbon (NCP) and inorganic calcium carbonate ($CaCO_3$). NCP for each of the three sampling regions, calculated both to the seasonally varying mixed layer depth and to the winter ventilation depth, has previously been determined based on measurements of dissolved O_2/Ar gas ratios made on the same transects as carbonate chemistry measurements analyzed here (full details are in *Palevsky et al*. [2016b]). O_2/Ar samples for the NCP analysis were measured at most stations with carbonate chemistry measurements included in the analysis in this paper (88%), as well as at a number of additional locations ($n = 271$) along the same transects where carbonate chemistry measurements are not available. We use NCP rates determined at all sampling locations with O_2/Ar because NCP rates determined only from the locations with carbonate chemistry samples differ minimally from those calculated from the full data set over the spring through fall productive season (differences of 0–10%, all well within the uncertainty bounds of the NCP estimates).

Since spatial and temporal variability in our study regions precludes direct estimation of $CaCO_3$ production rates from DIC and TA mass balance, we use $CaCO_3$ production rates based on published estimates of the particulate inorganic carbon (PIC):particulate organic carbon (POC) ratio and O_2/Ar-based regional estimates of NCP. We assume PIC:POC ratios of 0.1, 0.2, and 0.3 for the Kuroshio, Western, and Eastern regions, respectively. PIC:POC for the Kuroshio region is based on recent observational estimates at the Kuroshio Extension Observatory [*Fassbender*, 2014], which also match estimates of the global mean PIC:POC ratio [*Jin et al*., 2006] and are consistent with previous regional analysis indicating low calcification rates in the western North Pacific [*Wong et al*., 2002]. Observational estimates in the eastern subarctic North Pacific have found PIC:POC ratios above the global mean, with the mean value of 0.3 for the Eastern region taken from multiple observation-based estimates at Ocean Station Papa [*Fassbender et al*., 2016]. We assume an intermediate value for the Western region (0.2), where region-specific observational estimates are lacking. Multiplying these PIC:POC ratios by O_2/Ar-based seasonal NCP rates in each region yields estimated rates of $CaCO_3$ production of 0.4, 0.7, and 0.9 mol m^{-2} yr^{-1} in the Kuroshio, Western, and Eastern regions, respectively. This approach implicitly assumes that all NCP is exported as POC rather than as dissolved organic carbon which likely overestimates $CaCO_3$ export (since dissolved organic carbon contributes on order ~20% to global NCP) [*Hansell and Carlson*, 1998], but the uncertainty in this assumption is less than that in the PIC:POC values. We assume 100% uncertainty in estimated seasonal $CaCO_3$ production rates for all regions.

3.2.4. Uncertainty Analysis

We quantify uncertainty in each term in equations (1) and (2) resulting from both methodological error and undersampling bias. Methodological uncertainties in seasonal and regional mean carbonate chemistry, the time rate of change terms, and air-sea CO_2 flux rates are described above. Sampling bias is calculated based on comparison between regional mean satellite-based SST and chlorophyll concentrations for each season determined only from the times and cruise track locations where discrete samples were collected and those determined using all grid points within each region sampled continuously from 2008 to 2012 (Moderate Resolution Imaging Spectroradiometer 1/6° × 1/6° monthly data provided by the Oregon State Ocean Productivity group, http://www.science.oregonstate.edu/ocean.productivity). This is the approach used previously by *Palevsky et al*. [2016b] to determine sampling bias in NCP estimates. Sampling biases for the set of sampling locations with carbonate chemistry data used in this analysis are similar to those found in the O_2/Ar discrete sampling dataset evaluated by *Palevsky et al*. [2016b] (Figure S3). Undersampling bias in our estimates of air-sea CO_2 flux and in the time rate of change of both DIC and pCO_2 is calculated as the mean percent difference between satellite-based SST and chlorophyll concentrations calculated over the entire region and season versus those calculated using only the times and locations of our discrete sample collection. Undersampling bias in temperature and salinity effects on pCO_2 (equation (3)) are calculated solely from the mean percent difference between fully sampled and discrete sample-based SST. The combined effects of uncertainty in carbonate chemistry estimates and in gas exchange, NCP, and $CaCO_3$ production rates in equations (5)–(7) are propagated following standard analytical formulas. The magnitude of DIC physical supply is

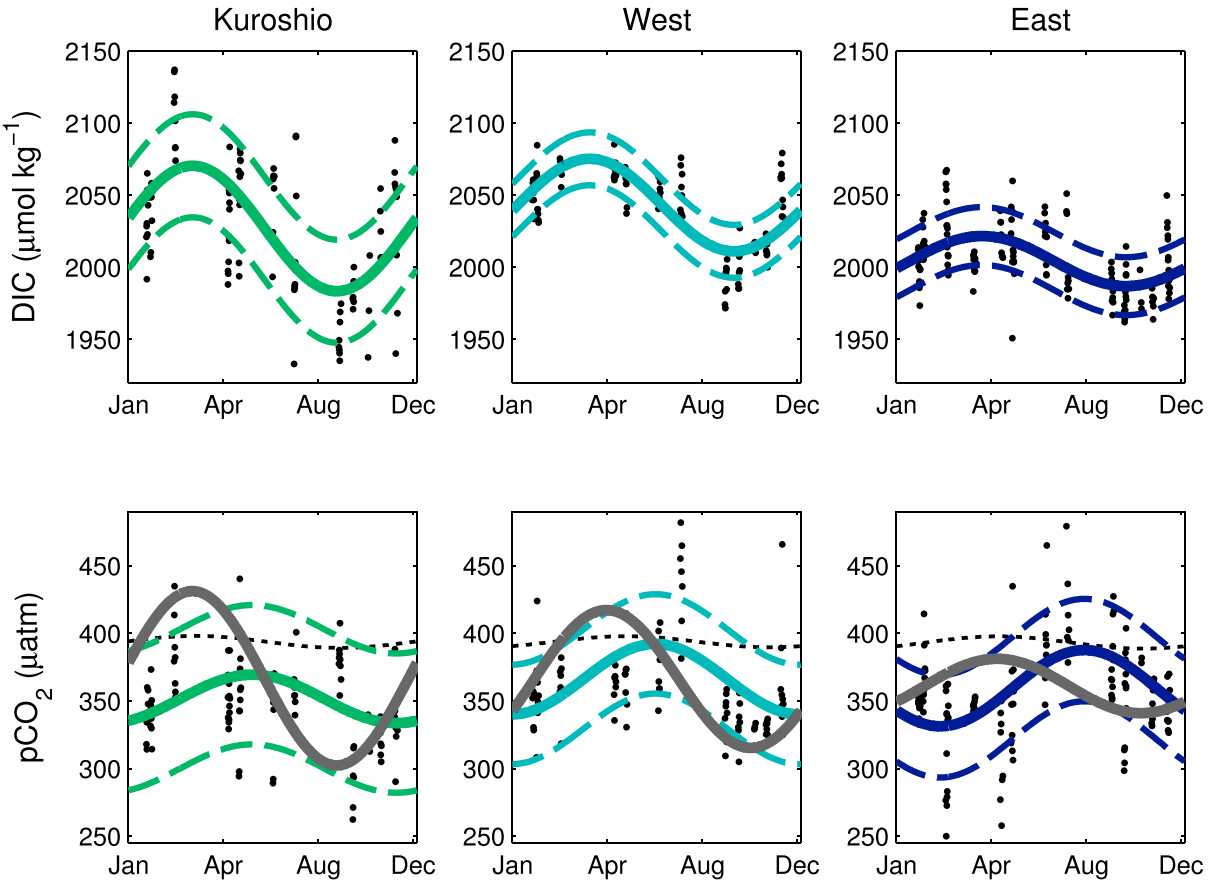

Figure 2. Composite annual cycle for (top row) DIC and (bottom row) seawater pCO_2 in each region. Black dots show all discrete sample measurements in a given region (two samples with $pCO_2 < 250$ μatm and seven samples with $pCO_2 > 500$ μatm are outside the *y* axis bounds). The solid colored lines are harmonic fits describing the annual cycle and the dashed colored lines show the harmonic fit ± root-mean-square error. For pCO_2, the solid gray line shows the pCO_2 seasonal cycle normalized to mean annual SST for each region and the dashed black line shows atmospheric pCO_2.

determined as the residual term in both equations (1) and (2), and the error in this term is determined by propagating error from each individual term.

4. Results and Discussion

4.1. Seasonal Cycle of DIC and pCO_2

DIC concentrations in the mixed layer show similar seasonal cycle timing in all three regions, with an annual maximum in spring and a minimum in fall (Figure 2 and Table 1). This is consistent with biological removal of DIC during the spring through fall productive season and physical supply of DIC from winter mixing and vertical diffusion. The amplitude of the DIC seasonal cycle increases westward across the basin, consistent with westward increases in both summertime NCP and winter mixed layer depths and with previous observations in the region [*Wong et al.*, 2002].

Mixed layer pCO_2 is lower than atmospheric pCO_2 (394 ± 5 μatm) for the majority of the year in all three regions and follows a seasonal cycle offset from that of DIC, with a maximum in summer and minimum in winter (Figure 2 and Table 1). Variability of individual discrete sample measurements around the mean seasonal cycle is greater for pCO_2 than for DIC and, in contrast to DIC, the seasonal cycle amplitude for pCO_2 is lower in the Kuroshio region than the West and East (amplitudes in the Kuroshio, West, and East, respectively, are 36 ± 51, 52 ± 37, and 56 ± 38 μatm for pCO_2 and 87 ± 36, 64 ± 18, and 35 ± 20 μmol kg^{-1} for DIC). Previous global-scale analysis has demonstrated that pCO_2 seasonal cycles reflect the combined effects of two offsetting processes: temperature effects which increase pCO_2 during summertime and

Table 1. Summary of Regional Mean Carbonate Chemistry and Air-Sea CO_2 Flux Rates Across the North Pacific[a]

	No. of Samples	DIC[b] (μmol kg^{-1})	TA[b] (μmol kg^{-1})	pCO_2[b] (μatm)	Air-Sea CO_2 flux[c]
		Kuroshio (142°E–170°E)			
Spring (MAM)	24	2042 ± 1 (31)	2264 ± 1 (18)	360 ± 4 (43)	5.7 ± 2.5
Summer (JJA)	17	2026 ± 1 (45)	2239 ± 1 (18)	371 ± 3 (101)	0.9 ± 0.4
Fall (SON)	27	1982 ± 1 (31)	2237 ± 2 (17)	333 ± 2 (38)	8.7 ± 5.2
Winter (DJF)	36	2051 ± 1 (42)	2255 ± 1 (25)	348 ± 2 (28)	14.8 ± 2.6
Annual	104				2.7 ± 0.9
		West (170°E–160°W)			
Spring (MAM)	27	2065 ± 1 (10)	2230 ± 1 (16)	364 ± 3 (19)	6.8 ± 1.6
Summer (JJA)	17	2051 ± 1 (13)	2205 ± 1 (8)	420 ± 4 (57)	−2.4 ± 0.7
Fall (SON)	27	2001 ± 1 (14)	2222 ± 1 (17)	227 ± 2 (15)	10.2 ± 1.7
Winter (DJF)	27	2052 ± 1 (15)	2237 ± 1 (21)	356 ± 3 (30)	10.6 ± 2.1
Annual	98				2.3 ± 0.4
		East (160°W–125°W)			
Spring (MAM)	50	2017 ± 1 (23)	2225 ± 1 (21)	332 ± 2 (37)	11.0 ± 1.6
Summer (JJA)	20	2012 ± 1 (23)	2201 ± 1 (7)	414 ± 4 (54)	−1.0 ± 0.3
Fall (SON)	39	1982 ± 1 (12)	2208 ± 2 (8)	363 ± 3 (28)	4.6 ± 1.0
Winter (DJF)	36	2007 ± 1 (18)	2213 ± 1 (19)	353 ± 2 (17)	8.8 ± 1.5
Annual	145				2.1 ± 0.3

[a]MAM = March–May, JJA = June–August, SON = September–November, and DJF = December–February.
[b]Results are given as mean ± uncertainty, reflecting methodological error in individual measurements. 1σ variability about the mean is given in parentheses, reflecting regional variability.
[c]Seasonal rates for air-sea CO_2 flux are given in mmol C m^{-2} d^{-1} and annual rates are in mol C m^{-2} yr^{-1}. Results are given as mean ± uncertainty, reflecting both methodological error and sampling bias (see text for details).

decrease pCO_2 during wintertime, and non-temperature effects which decrease pCO_2 during summer due to biological drawdown and increase pCO_2 in winter due to vertical physical supply of high-pCO_2 waters, with temperature effects dominating in the subtropics and non-temperature effects dominating in the subarctic North Pacific [*Takahashi et al.*, 2002]. Our observed pCO_2 seasonal cycle reflects the competing effects of both processes at the interface between the subtropical and subarctic regimes which both mute the amplitude of the seasonal cycle and increase variability.

To evaluate the pCO_2 seasonal cycle independent of the temperature effect we calculate the temperature-normalized pCO_2 seasonal cycle at the mean annual SST for each region (Figure 2, calculated following equation (1) from *Takahashi et al.* [2002]: pCO_2 at $T_{mean} = pCO_{2,obs} \times \exp[0.0423(T_{mean} - T_{obs})]$, where "obs" and "mean" indicate the observed and annual mean values, respectively). The coincident seasonal cycles in temperature-normalized pCO_2 and DIC (Figure 2) imply that the lag between the pCO_2 and DIC maxima results from the temperature effect on pCO_2. Furthermore, the westward increase in the amplitudes of DIC and temperature-normalized pCO_2 indicates that the non-temperature effects on pCO_2 are caused by the same processes causing seasonal changes in DIC.

4.2. Factors Influencing the Seasonal Cycle of Mixed Layer DIC and pCO_2

To quantitatively evaluate the factors influencing the observed seasonal cycles in mixed layer DIC and pCO_2, we consider the role of each component term in equations (1) and (2) for DIC and pCO_2, respectively (Figure 3). Air-sea CO_2 flux drives a small but steady increase in mixed layer DIC and pCO_2 via net uptake of atmospheric CO_2 throughout the year except in summer in the Western and Eastern regions, when the ocean outgases CO_2. NCP is the primary factor driving spring through fall decreases in both DIC and pCO_2. While both NCP and $CaCO_3$ production lead to a net removal of DIC, $CaCO_3$ production causes a net increase in pCO_2 by decreasing TA in a 2:1 ratio to DIC. However, even in the East with the largest specified PIC:NCP ratio across the basin of 0.3, $CaCO_3$ production only offsets ~20% of the pCO_2 drawdown due to NCP. The temperature effect increases pCO_2 during periods of warming in spring and summer and decreases pCO_2 during fall and winter cooling. The large temperature-driven increase in pCO_2 during summer largely offsets the NCP-driven pCO_2 drawdown, consistent with previous analysis of regional pCO_2 observations [*Chierici et al.*, 2006]. The westward increasing seasonal cycle in SST amplifies the offset in tandem with westward increasing productive season NCP rates and produces a lower amplitude seasonal cycle in observed pCO_2 than in DIC

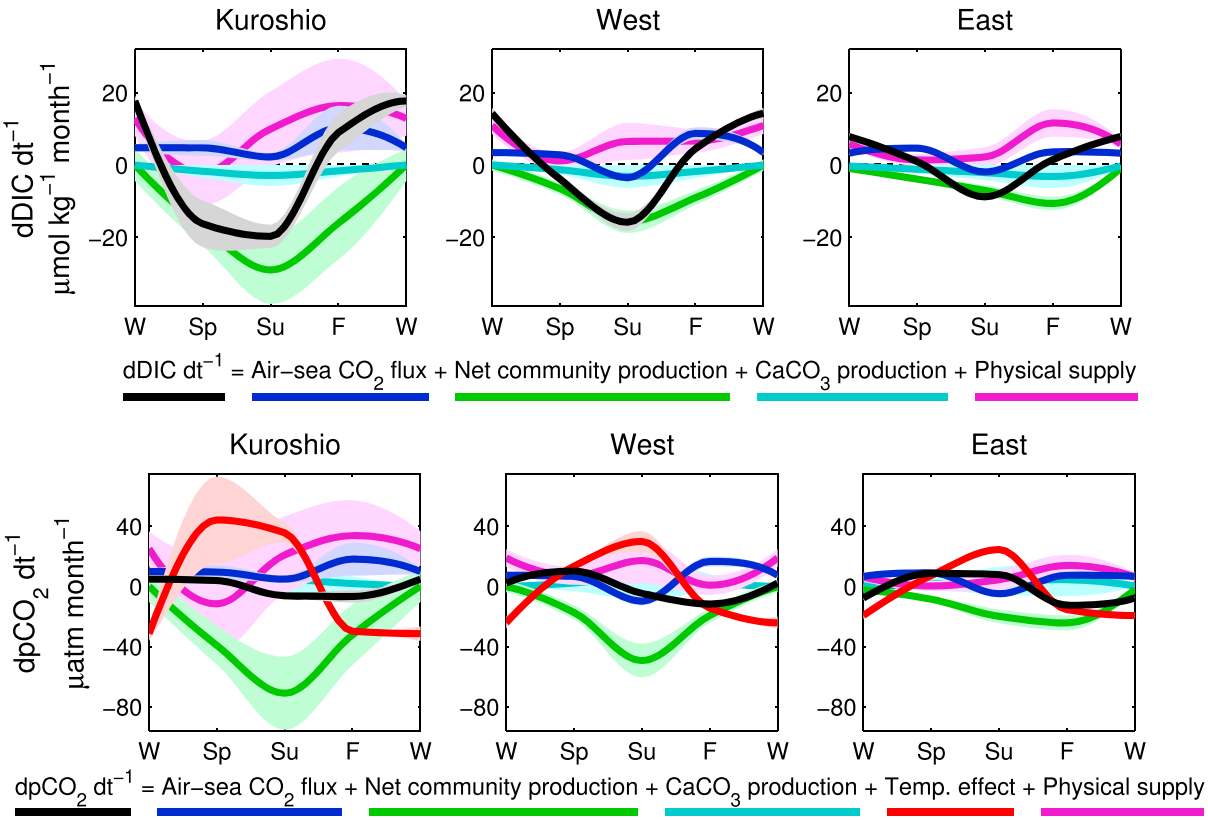

Figure 3. Seasonal influences on (top row) DIC concentrations and (bottom row) seawater pCO_2 in the surface mixed layer in each region, calculated following equations (1) and (2), respectively. Positive (negative) values represent increases (decreases) in mixed layer DIC and pCO_2. The salinity effect on seawater pCO_2 is negligible and is omitted for clarity.

(Figure 2). The effect of seasonal changes in salinity on pCO_2 is negligible and therefore not shown in Figure 3 or further discussed in the results.

Seasonal changes in mixed layer depth (Figure S4) vary the effect of air-sea and biological carbon fluxes on mixed layer DIC concentrations and pCO_2, with effects amplified during the stratified summer season when there is a smaller volume of water in the mixed layer and dampened in the winter when there is a larger volume of water in the mixed layer. Therefore, even though the rate of air-sea CO_2 flux is greatest in winter in the Kuroshio and Western regions, its influence on DIC and pCO_2 in winter is less than half that in fall because winter mixed layer depths are 2–4 times deeper. Similarly, the influence of biological removal of DIC via NCP is enhanced in the summer even though NCP rates per square meter are greater in spring and fall than in summer.

Seasonal patterns of physical supply, calculated as the residual term in both equations (1) and (2), are similar for DIC and pCO_2 (Figure 3). Broadly, this seasonal pattern shows a minimum in physical supply of DIC and pCO_2 to the mixed layer in spring and a maximum in fall to winter. TA physical supply (Figure S5) also shows a similar seasonal pattern of physical supply, though with lower amplitude. The physical supply term includes both horizontal advection due to geostrophic and Ekman-driven transport as well as vertical supply from diffusive mixing, entrainment, and upwelling. Our approach cannot distinguish the contributions of each of these individual processes, so for context we turn to previous work in the North Pacific transition zone region by *Ayers and Lozier* [2012]. Their work demonstrated that vertical supply of high-DIC waters increases mixed layer pCO_2 during the period of intense entrainment and vertical diffusion from late fall through early spring [*Ayers and Lozier*, 2012]. Horizontal advective transport has steady effects throughout the year in the transition zone region, with Ekman transport supplying high-DIC waters from the north and geostrophic transport by the Kuroshio and Kuroshio Extension currents supplying low-DIC waters that reduce mixed layer DIC and pCO_2 in the region [*Ayers and Lozier*, 2012]. Although our calculations of physical supply as a residual term

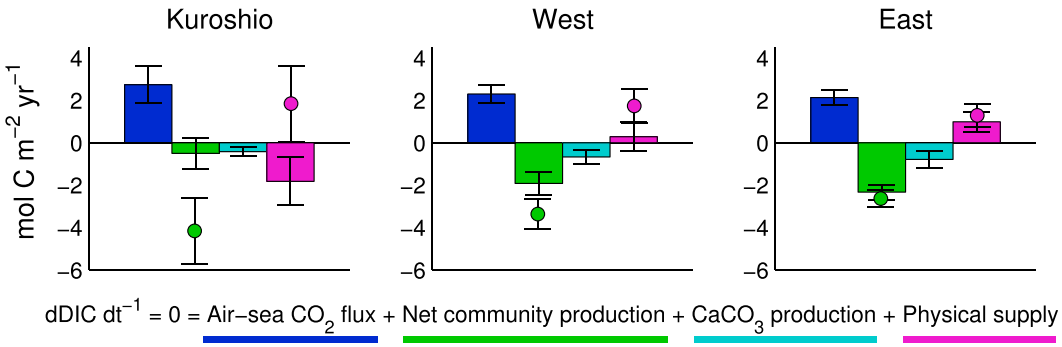

Figure 4. Annual DIC budget for each region, calculated following equation (1). Positive (negative) values represent increases (decreases) in surface ocean DIC. Note the differing influences of NCP and physical supply on the DIC budget integrated to the winter ventilation depth (bars) compared to the DIC budget integrated to the base of the seasonally varying mixed layer depth (filled circles). See text for discussion.

cannot separate these individual processes, our overall seasonal cycle of physical supply matches that found by summing all the physical effects considered by *Ayers and Lozier* [2012], indicating that we have adequately captured the key physical influences on DIC and pCO_2 in this region.

4.3. Factors Influencing the Annual DIC Budget

Annual influences on DIC are calculated following equation (1) assuming that over a composite annual cycle $\frac{\partial DIC}{\partial t} \approx 0$. Annual flux rates are determined for each RHS term in equation (1), with two separate DIC budgets calculated integrating, first, to the base of the seasonally varying mixed layer depth and, second, to the winter ventilation depth. Note that the only two terms that differ between these two depth criteria are NCP and the residual physical supply term.

Air-sea CO_2 flux leads to a net annual increase in ocean DIC inventory in all three regions, with rates of 2.7 ± 0.9, 2.3 ± 0.4, and 2.1 ± 0.3 mol C m^{-2} yr^{-1} in the Kuroshio, Western, and Eastern regions, respectively. These rates are consistent with the spatial trend of westward intensified ocean CO_2 uptake across the basin identified by *Takahashi et al.* [2009] (Figure 1) but are ~0.6–0.9 mol C m^{-2} yr^{-1} (~30–60%) greater than the rates determined by *Takahashi et al.* [2009]. The decade-long interval between the *Takahashi et al.* [2009] reference year of 2000 and the 2008–2012 sampling period of our study is not long enough to distinguish potential strengthening of the ocean carbon sink from natural variability [*McKinley et al.*, 2016]. Differences between our estimates and those of *Takahashi et al.* [2009] may also result from interpolation choices in developing the global climatology or from differences in the choice of air-sea gas transfer parameterizations, as well as actual differences between the measurement time periods.

We account for the effect of winter ventilation on the annual DIC budget by comparing budget terms integrated to the winter ventilation depth and those integrated to the seasonally varying mixed layer depth (Figure 4). If the annual DIC inventory is computed to the base of the seasonally varying mixed layer (colored circles in Figure 4), biological export of organic carbon (NCP) removes sufficient DIC to more than counterbalance the annual DIC increase due to air-sea CO_2 flux. However, integrating the DIC budget to a constant winter ventilation depth for each region paints a different picture. Although organic carbon export from the stratified mixed layer in spring through fall is greatest in the Kuroshio and decreases eastward across the basin, much of this organic material is remineralized below the base of the seasonally stratified mixed layer and reenters the mixed layer during deep winter mixing in the western basin, ventilating it to the atmosphere [*Palevsky et al.*, 2016b]. Estimates of annual NCP are significantly reduced in the Kuroshio and Western regions when accounting for winter ventilation, whereas the reduction is small in the Eastern region due a strong permanent halocline that prevents winter mixing below ~120 m (green bars in Figure 4).

When accounting for the effect of winter ventilation in the annual DIC budget, it becomes clear that the relative roles of NCP and of physical supply of DIC vary considerably across the basin (illustrated in Figure 5, which highlights the key processes from the DIC budget in Figure 4). NCP remains more than able to counterbalance the DIC increase due to air-sea CO_2 flux in the East. In the Kuroshio region, by contrast,

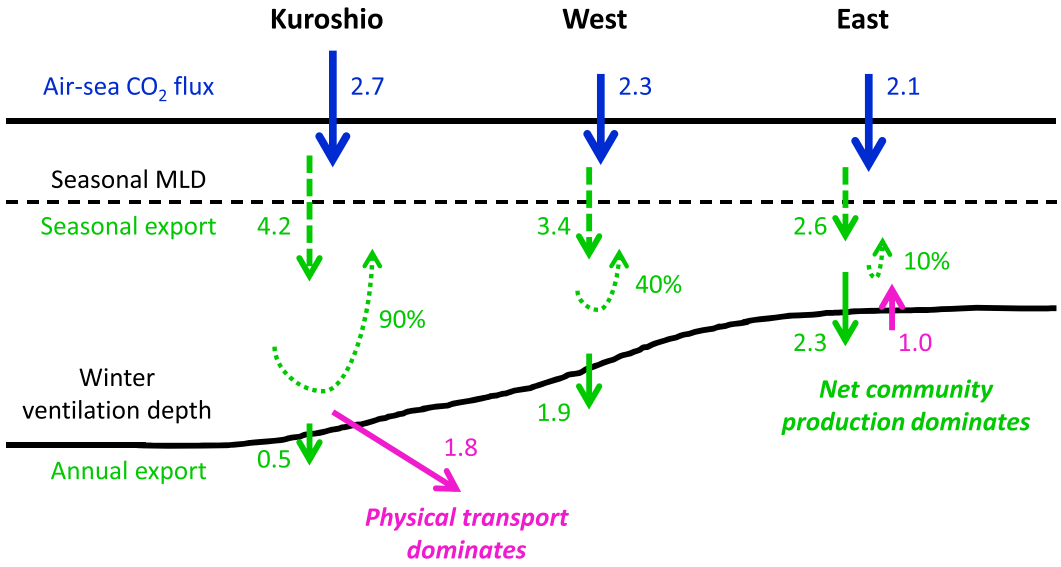

Figure 5. Schematic representation of the key processes in the annual DIC budget (Figure 4). All numbers represent annual carbon fluxes in mol C m^{-2} yr^{-1}. Seasonal export represents NCP integrated to the seasonally varying mixed layer depth, while annual export represents NCP integrated to the winter ventilation depth, with the percent of seasonal export remineralized above the winter ventilation depth depicted in each region. Annual physical supply in the Kuroshio and East is shown in purple. $CaCO_3$ production and physical transport in the West are omitted for clarity.

~90% of seasonal NCP is remineralized and ventilated back to the atmosphere such that the fraction of NCP that remains sequestered on an annual basis can only counterbalance a small fraction of the DIC increase due to air-sea CO_2 flux. As a result, physical processes must counterbalance the CO_2 input from gas exchange in the Kuroshio region. According to analysis by *Ayers and Lozier* [2012], the only physical process that leads to a net removal of DIC in this region is geostrophic advection, which transports low-DIC subtropical waters northward into the region via the Kuroshio Current and exports high-DIC waters eastward via the Kuroshio Extension. All other physical processes, including Ekman transport and vertical supply via entrainment, diffusive mixing and upwelling, yield a net supply of DIC. Our calculated physical supply term (residual in equation (1)) represents the net result of all physical processes. Across the basin, the role of physical processes changes from being a net DIC sink in the west to a net DIC source in the east (Figure 4), which follows the eastward decrease in the strength of geostrophic transport by the Kuroshio Extension.

The influence of $CaCO_3$ production on the DIC budget presented here assumes that none of the $CaCO_3$ exported from the seasonally stratified mixed layer dissolves above the winter ventilation depth. Despite expected faster sinking of $CaCO_3$-ballasted particles [*Armstrong et al.*, 2002; *Klaas and Archer*, 2002], this is likely an overestimate of the contribution from $CaCO_3$ production to the annual DIC budget, since recent sediment trap measurements in the western subarctic gyre show a decrease in $CaCO_3$ flux between 60 and 200 m, likely driven by shallow aragonite and calcite saturation depths at 100 m and 200 m, respectively [*Honda et al.*, 2015]. However, even without allowing for dissolution of sinking $CaCO_3$ particles, $CaCO_3$ production provides a fairly minor contribution to the annual DIC budget. TA removal by $CaCO_3$ production is the dominant term in the annual TA budget (Figure S5), indicating the need for improved constraint on $CaCO_3$ production rates to assess the role of TA physical supply in the region.

4.4. Factors Influencing Annual Mixed Layer pCO_2

Annual influences on pCO_2 are calculated following equation (2) assuming that over a composite annual cycle $\frac{\partial pCO_2}{\partial t} \approx 0$. This simplifying assumption is justified because rates of surface water pCO_2 increase in the North Pacific are $< 3\,\mu atm\,yr^{-1}$ [*Takahashi et al.*, 2009], which is negligible given the magnitude of other terms (Figure 6). Annual influences on mixed layer pCO_2 are determined for each RHS term in equation (2), with the roles of NCP and physical supply calculated both with and without accounting for winter ventilation (Figure 6), as in the annual DIC budget (Figure 4). Note that this calculation is not a mass balance budget, as

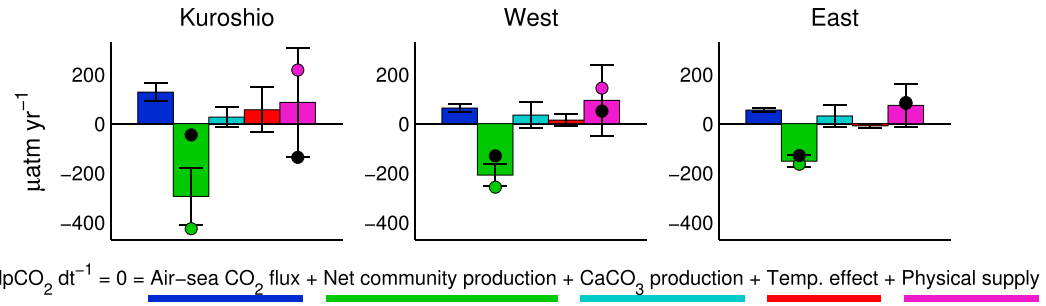

Figure 6. Annual influences on pCO_2 in the surface mixed layer in each region, calculated following equation (2). Positive (negative) values represent increases (decreases) in mixed layer pCO_2. The salinity effect is negligible and is omitted for clarity. The colored circles for NCP and physical supply integrate effects on the surface mixed layer shown in Figure 3. The colored bars account for winter ventilation, with a best estimate of when that ventilation occurs based on seasonal entrainment rates (see text for details). The black dots represent a thought experiment scenario where the total annual NCP rate is equivalent to the winter ventilation estimate shown in the colored bars, but results from reduced productive season NCP rather than winter ventilation.

computed for DIC, but instead reflects cumulative effects of seasonal influences on pCO_2 throughout the year. The only terms that differ when accounting for winter ventilation are NCP and the residual physical supply term, as was the case for the DIC budget.

It is important to note that the impact of a given carbon flux on mixed layer pCO_2 depends on mixed layer depth because the pCO_2 change depends on the DIC concentration change (via equation (8)) and the DIC concentration change depends inversely on mixed layer depth, as described in section 4.2. Thus, a given NCP flux out of the shallow stratified mixed layer in summer decreases the pCO_2 more than the return of this same flux (as DIC) into a deep mixed layer in winter increases the pCO_2. This mixed layer depth effect weights the annual pCO_2 cycle toward summertime NCP and away from wintertime DIC supply via vertical mixing and entrainment that ventilates remineralized organic carbon. We approximate the timing of winter ventilation based on seasonal entrainment rates in each season, which indicate that ~30% of ventilation occurs during initial mixed layer deepening in fall and 10–20% occurs during continued entrainment in early spring in the West and East, while the dominant remainder of ventilation occurs during winter. This ventilation lessens the annual impact of NCP on pCO_2 as compared with the estimate not accounting for ventilation of remineralized seasonally exported carbon (green bars as compared with green filled circles in Figure 6). However, despite ventilation of 90% and 40% of seasonally exported carbon in the Kuroshio and Western regions respectively, the reductions in the influence of NCP on annual drawdown of surface ocean pCO_2 are only 30% and 20%, respectively. This strong effect of seasonal timing on the ability of NCP to influence surface ocean pCO_2 is due to the seasonal cycle of mixed layer depths, where winter mixed layers are 8 times deeper than summer mixed layers in the Kuroshio and 5 times deeper in the West and East (Figure S4).

To further illustrate the importance of seasonal timing, we conduct a thought experiment in which the total annual NCP rate determined at the winter ventilation depth is unchanged but the NCP timing is redistributed seasonally. In this thought experiment, rather than allowing organic material to be seasonally exported and subsequently remineralized and ventilated as mixed layers deepen, NCP rates are proportionally reduced from spring through fall (black circles in Figure 6). This scenario significantly diminishes the ability of NCP to reduce surface ocean pCO_2 on an annual basis, although the total annual NCP flux is unchanged from that in the more realistic ventilation-based calculation of the influence of NCP (green bars in Figure 6). The thought experiment scenario therefore requires greater removal of pCO_2 by physical processes. Since both scenarios are based on the same annual NCP flux rate, both are consistent with the DIC budget accounting for the effects of winter ventilation (colored bars in Figure 4) despite their differing effects on pCO_2. This thought experiment, though unrealistic, demonstrates that knowledge of the timing of export and ventilation, as well as the rates, is important for quantifying the influence of NCP and ventilation on mixed layer pCO_2 and thus on the air-sea CO_2 flux.

Our analysis indicates that export of organic material (NCP) is the primary process drawing down pCO_2 in the three regions (Figure 6) although the magnitude of its importance depends on the timing of the physical processes ventilating remineralized organic matter back to the mixed layer as DIC, as discussed above. Our

estimates indicate that physical processes cause a net annual increase in pCO_2 in all three regions (86 ± 222, 95 ± 145, and 74 ± 86 μatm yr^{-1} in the Kuroshio, Western, and Eastern regions, respectively), albeit with large uncertainties since physical supply is calculated as the residual in equation (2) with uncertainty therefore depending on errors in all other terms, including significant uncertainty in seasonal MLD estimates. These results are consistent with those of *Ayers and Lozier* [2012] who estimated that physical processes cause a net pCO_2 increase of 59 ± 17 μatm yr^{-1} in the transition zone, with pCO_2 increases from Ekman transport and vertical mixing/entrainment more than counteracting the pCO_2 decrease from geostrophic advection.

The influence of $CaCO_3$ production on pCO_2 is substantially smaller than the influence of NCP and physical processes (Figure 6). However, it does drive a biological counterpump that annually increases surface ocean pCO_2 at more than half the rate of air-sea CO_2 flux in the Eastern and Western regions. Improved estimates of the rate of $CaCO_3$ production are needed to constrain widely varying literature values and predict potential future changes in $CaCO_3$ production that could influence the strength of the North Pacific Ocean carbon sink.

4.5. Effects of Seasonality on Annual Air-Sea CO_2 Flux

Assessing the drivers of air-sea CO_2 flux requires us to consider not only the annual changes in surface ocean pCO_2 (Figure 6) but also the effect of those pCO_2 changes in driving CO_2 exchange between the surface ocean and atmosphere. Wintertime increases in CO_2 solubility and wind speed-dependent air-sea gas transfer rates (K_0 and k_{CO_2}, respectively, in equation (10)) enhance the leverage of winter over summer pCO_2 changes in driving air-sea CO_2 flux by 4 times, 2.7 times, and 2.9 times in the Kuroshio, Western, and Eastern regions, respectively. This gas exchange effect, dominated by wind speed-driven changes in k_{CO_2}, interacts with the effects of seasonality in mixed layer depth and in biological export and ventilation described in sections 4.2 and 4.4 as well as the effects of seasonal SST changes on pCO_2.

Although the temperature effect is an important influence on the pCO_2 seasonal cycle (Figure 3), its influence on pCO_2 over an annual basis is indistinguishable from zero in all regions (Figure 6). This result is consistent with previous analysis of climatological pCO_2 in the North Pacific transition zone [*Ayers and Lozier*, 2012]. Nevertheless, wintertime increases in K_0 and k_{CO_2} magnify the influence of winter temperature-driven decreases in pCO_2 on annual air-sea CO_2 flux rates. If K_0 and k_{CO_2} were held constant at the annual mean in each region, annual air-sea CO_2 flux would be reduced to 91%, 78%, and 73% of the actual rates in the Kuroshio, Western, and Eastern regions, respectively. These potential reductions are similar to those previously estimated for the full transition zone region [*Ayers and Lozier*, 2012].

In addition to enabling temperature-based solubility changes to drive a portion of the annual ocean carbon sink, seasonal asymmetries in the leverage of surface ocean pCO_2 on air-sea CO_2 flux also partially offset the effects of seasonality in mixed layer depth and NCP timing. Although NCP-driven carbon fluxes from the shallow summertime mixed layer exert an enhanced influence on pCO_2, the ability of this biological carbon export to drive air-sea CO_2 flux is reduced due to lower summertime K_0 and k_{CO_2}. Similarly, although remineralized organic carbon ventilated during winter has a reduced influence on pCO_2 due to deep wintertime mixed layers, pCO_2 changes resulting from this ventilation have an enhanced influence on air-sea CO_2 flux due to higher wintertime K_0 and k_{CO_2}. Seasonal timing is thus important not only in determining the influence of carbon fluxes on surface ocean pCO_2 but also in determining the influence of pCO_2 changes in driving air-sea CO_2 flux.

5. Conclusions

In this study, we have combined measurements of the complete carbonate chemistry system across the North Pacific basin throughout the full annual cycle with previously described estimates of NCP based on O_2/Ar measurements [*Palevsky et al.*, 2016b] to investigate the relative roles of chemical, physical, and biological processes in driving uptake of atmospheric CO_2. Air-sea CO_2 exchange is an atmospheric CO_2 sink (and source of DIC to the surface ocean) across the North Pacific basin. We find that the annual SST cycle has a strong effect on the seasonal pCO_2 cycle (Figures 2 and 3) but little effect on annual changes in surface ocean pCO_2 (Figure 6) and can account for less than 25% of each region's annual air-sea CO_2 flux, requiring that physical and biological processes drive annual ocean CO_2 uptake.

The annual DIC budget (Figures 4 and 5) shows an east-west trend across the basin with physical circulation processes as the dominant DIC sink in the Kuroshio region and NCP as the dominant DIC sink in the East. This spatial trend is only apparent when accounting for annual rates of NCP calculated to the winter ventilation depth, which reveal that ~90% of the seasonally exported organic carbon in the Kuroshio region is subsequently remineralized and entrained into the mixed layer as DIC during deep winter mixing. Without accounting for winter ventilation, we would overestimate the influence of vertical DIC supply by counting this ventilation of remineralized carbon as a physical influence rather than a reduction in annual NCP. The effects of winter ventilation on surface ocean pCO_2 are still substantial but more muted (Figure 6). The influence of annual NCP on surface ocean pCO_2 depends not only on the magnitude of the annual flux but also on its timing, since an identical flux has a larger influence on mixed layer DIC concentrations and thus pCO_2 when exported from a shallow summer mixed layer than a deep winter mixed layer.

Annual air-sea CO_2 flux increases westward across the basin, from 2.1 ± 0.3 mol C m^{-2} yr^{-1} in the East to 2.7 ± 0.9 mol C m^{-2} yr^{-1} in the Kuroshio region. These rates are 4–5 times the global mean rate of ocean carbon uptake, underscoring the previously recognized role of the North Pacific as a significant sink of atmospheric CO_2 [*Takahashi et al*., 2009]. Repeated sampling of this region over the coming decades will be necessary to resolve potential changes to the strength of the region's ocean carbon sink, with expected time of emergence for climate-driven changes to air-sea CO_2 flux in the seasonally stratified North Pacific in 2040–2060 [*McKinley et al*., 2016]. We demonstrate that the biological pump (NCP) plays a key role in driving the North Pacific Ocean carbon sink and also that the influence of NCP on air-sea CO_2 flux depends not only on the magnitude of organic material export rates but also on the magnitude and timing of mixed layer deepening during fall and winter and the seasonal cycle in wind speed-driven gas exchange. Seasonal variations in NCP, mixed layer depth, and wind speed have a particularly strong impact on ocean CO_2 uptake in high-latitude regions with a strong seasonal cycle such as the Kuroshio, where deep winter mixed layers return a significant fraction of exported organic carbon to the surface ocean, and ultimately atmosphere, as CO_2. Thus, future studies aiming at unraveling the role of the biological pump in driving the ocean CO_2 sink [e.g., *Siegel et al*., 2016] need to not only focus on estimating the annual NCP rate but also account for the timing of seasonal export and impact of winter ventilation.

Acknowledgments
All container ship carbonate chemistry measurements are available from the Biological & Chemical Oceanography Data Management Office (http://www.bco-dmo.org/dataset/665195). Additional publicly available data sources are listed where described in section 3. We thank the Orient Overseas Container Line (OOCL) and the captains and crew of the M/V *OOCL Tokyo* and M/V *OOCL Tianjin* for their assistance and gracious hospitality at sea; Deirdre Lockwood, Johnny Stutsman, and Mark Haught for assistance with field sampling; Johnny Stutsman, Mariela R. T. White, and Alison Barner for assistance with DIC measurements; Cathy Cosca for processing underway pCO_2 data; Dave Munro for assistance in using CarbonTracker data; and Curtis Deutsch, Steve Emerson, and two anonymous reviewers for providing constructive feedback that improved the manuscript. This work was funded by a NDSEG Fellowship from the Office of Naval Research, a NSF Graduate Research Fellowship and an ARCS Foundation Fellowship to H.I.P., by NSF Ocean Sciences (0628663 and 1259055 to P.D.Q), and by the NOAA Climate Program Office (A10OAR4310088 to P.D.Q.).

References

Anderson, L. A., and J. L. Sarmiento (1994), Redfield ratios of remineralization determined by nutrient data analysis, *Global Biogeochem. Cycles*, *8*(1), 65–80.

Armstrong, R. A., C. Lee, J. I. Hedges, S. Honjo, and S. G. Wakeham (2002), A new, mechanistic model for organic carbon fluxes in the ocean based on the quantitative association of POC with ballast minerals, *Deep Sea Res., Part II*, *49*, 219–236.

Ayers, J. M., and M. S. Lozier (2010), Physical controls on the seasonal migration of the North Pacific transition zone chlorophyll front, *J. Geophys. Res.*, *115*, C05001, doi:10.1029/2009JC005596.

Ayers, J. M., and M. S. Lozier (2012), Unraveling dynamical controls on the North Pacific carbon sink, *J. Geophys. Res.*, *117*, C01017, doi:10.1029/2011JC007368.

Chierici, M., A. Fransson, and Y. Nojiri (2006), Biogeochemical processes as drivers of surface fCO_2 in contrasting provinces in the subarctic North Pacific Ocean, *Global Biogeochem. Cycles*, *20*, GB1009, doi:10.1029/2004GB002356.

Ciais, P., et al. (2013), Carbon and other biogeochemical cycles, in *Climate Change 2013—The Physical Science Basis*, edited by P. M. M. Stocker et al., pp. 465–570, Cambridge Univ. Press, Cambridge, U. K., and New York.

Dickson, A. G., and F. J. Millero (1987), A comparison of the equilibrium constants for the dissociation of carbonic acid in seawater media, *Deep Sea Res.*, *34*(10), 1733–1743, doi:10.1016/0198-0149(87)90021-5.

Dickson, A. G., C. L. Sabine, and J. R. Christian (2007), Guide to best practices for ocean CO_2 measurements, *PICES Spec. Publ.*, *3*, 191.

Fassbender, A. (2014), New approaches to study the marine carbon cycle, PhD thesis, Univ. of Washington, Seattle, Wash.

Fassbender, A. J., C. L. Sabine, and M. F. Cronin (2016), Net community production and calcification from 7 years of NOAA Station Papa Mooring measurements, *Global Biogeochem. Cycles*, *30*, 250–267, doi:10.1002/2015GB005205.

Feely, R. A., R. Wanninkhof, H. B. Milburn, C. E. Cosca, M. Stapp, and P. P. Murphy (1998), A new automated underway system for making high precision pCO_2 measurements onboard research ships, *Anal. Chim. Acta*, *377*, 185–191.

Hansell, D. A., and C. A. Carlson (1998), Net community production of dissolved organic carbon, *Global Biogeochem. Cycles*, *12*(3), 443–453, doi:10.1029/98GB01928.

Harrison, P., P. Boyd, D. Varela, S. Takeda, A. Shiomoto, and T. Odate (1999), Comparison of factors controlling phytoplankton productivity in the NE and NW subarctic Pacific gyres, *Prog. Ocean.*, *43*(2–4), 205–234.

Harrison, P., F. Whitney, A. Tsuda, H. Saito, and K. Tadokoro (2004), Nutrient and plankton dynamics in the NE and NW gyres of the subarctic Pacific Ocean, *J. Ocean.*, *60*, 93–117.

Hauck, J., et al. (2015), On the Southern Ocean CO_2 uptake and the role of the biological carbon pump in the 21st century, *Global Biogeochem. Cycles*, *29*, 1451–1470, doi:10.1002/2015GB005140.

Honda, M. C., et al. (2015), Comparison of sinking particles in the upper 200 m between subarctic station K2 and subtropical station S1 based on drifting sediment trap experiments, *J. Oceanogr.*, *72*, 373–386, doi:10.1007/s10872-015-0280-x.

Jayne, S. R., et al. (2009), The Kuroshio Extension and its recirculation gyres, *Deep Sea Res., Part I*, *56*, 2088–2099, doi:10.1016/j.dsr.2009.08.006.

Jin, X., N. Gruber, J. P. Dunne, J. L. Sarmiento, and R. A. Armstrong (2006), Diagnosing the contribution of phytoplankton functional groups to the production and export of particulate organic carbon, $CaCO_3$, and opal from global nutrient and alkalinity distributions, *Global Biogeochem. Cycles*, *20*, GB2015, doi:10.1029/2005GB002532.

Klaas, C., and D. E. Archer (2002), Association of sinking organic matter with various types of mineral ballast in the deep sea: Implications for the rain ratio, *Global Biogeochem. Cycles*, *16*(4), 1116, doi:10.1029/2001GB001765.

Landschützer, P., N. Gruber, D. C. E. Bakker, and U. Schuster (2014), Recent variability of the global ocean carbon sink, *Global Biogeochem. Cycles*, *28*, 927–949, doi:10.1002/2014GB004853.

Le Quéré, C., et al. (2015), Global Carbon Budget 2015, *Earth Syst. Sci. Data*, *7*, 349–396, doi:10.5194/essd-7-349-2015.

Liss, P. S., and L. Merlivat (1986), Air-sea gas exchange rates: Introduction and synthesis, in *The Role of Air-Sea Exchange in Geochemical Cycling*, edited by P. Buat-Menard, pp. 113–127, D. Reidel, Hingham, Mass.

McKinley, G. A., et al. (2006), North Pacific carbon cycle response to climate variability on seasonal to decadal timescales, *J. Geophys. Res.*, *111*, C07S06, doi:10.1029/2005JC003173.

McKinley, G. A., D. J. Pilcher, A. R. Fay, K. Lindsay, M. C. Long, and N. S. Lovenduski (2016), Timescales for detection of trends in the ocean carbon sink, *Nature*, *530*, 469–472, doi:10.1038/nature16958.

Mehrbach, C., C. H. Culberson, J. E. Hawley, and R. M. Pytkowicz (1973), Measurement of the apparent dissociation constants of carbonic acid in seawater at atmospheric pressure, *Limnol. Oceanogr.*, *18*, 897–907, doi:10.4319/lo.1973.18.6.0897.

Monterey, G., and S. Levitus (1997), Seasonal variability of the mixed layer depth for the world ocean, *NOAA Atlas NESDIS*, *14*(5), 96.

Nightingale, P. D., G. Malin, C. S. Law, A. J. Watson, P. S. Liss, M. I. Liddicoat, J. Boutin, and R. C. Upstill-Goddard (2000), In situ evaluation of air-sea gas exchange parameterizations using novel conservative and volatile tracers, *Global Biogeochem. Cycles*, *14*(1), 373–387.

Ohno, Y., N. Iwasaka, F. Kobashi, and Y. Sato (2009), Mixed layer depth climatology of the North Pacific, *J. Ocean.*, *65*, 1–16.

Palevsky, H. I., F. Ribalet, J. E. Swalwell, C. E. Cosca, E. D. Cokelet, R. A. Feely, E. V. Armbrust, and P. D. Quay (2013), The influence of net community production and phytoplankton community structure on CO_2 uptake in the Gulf of Alaska, *Global Biogeochem. Cycles*, *27*, 664–676, doi:10.1002/gbc.20058.

Palevsky, H. I., P. D. Quay, and D. P. Nicholson (2016a), Discrepant estimates of primary and export production from satellite algorithms, a biogeochemical model and geochemical tracer measurements in the North Pacific Ocean, *Geophys. Res. Lett.*, *43*, 8645–8653, doi:10.1002/2016GL070226.

Palevsky, H. I., P. D. Quay, D. E. Lockwood, and D. P. Nicholson (2016b), The annual cycle of gross primary production, net community production, and export efficiency across the North Pacific Ocean, *Global Biogeochem. Cycles*, *30*, 361–380, doi:10.1002/2015GB005318.

Pierrot, D., C. Neill, K. Sullivan, R. Castle, R. Wanninkhof, H. Luger, T. Johannessen, A. Olsen, R. A. Feely, and C. E. Cosca (2009), Recommendations for autonomous underway pCO_2 measuring systems and data-reduction routines, *Deep Sea Res., Part II*, *56*(8–10), 512–522, doi:10.1016/j.dsr2.2008.12.005.

Polovina, J. J. J., E. Howell, D. R. D. R. Kobayashi, and M. P. M. P. Seki (2001), The transition zone chlorophyll front, a dynamic global feature defining migration and forage habitat for marine resources, *Prog. Oceanogr.*, *49*, 469–483, doi:10.1016/S0079-6611(01)00036-2.

Quay, P., and J. Stutsman (2003), Surface layer carbon budget for the subtropical N. Pacific: d13C constraints at station ALOHA, *Deep Sea Res., Part I*, *50*, 1045–1061, doi:10.1016/S0967-0637(03)00116-X.

Reuer, M. K., B. A. Barnett, M. L. Bender, P. G. Falkowski, and M. B. Hendricks (2007), New estimates of Southern Ocean biological production rates from O_2/Ar ratios and the triple isotope composition of O2, *Deep Sea Res., Part I*, *54*, 951–974, doi:10.1016/j.dsr.2007.02.007.

Roden, G. I. (1991), Subarctic-subtropical transition zone of the North Pacific: Large-scale aspects and mesoscale structure, *NOAA Tech. Rep. NMFS*, *105*, 1–38.

Roy, T., L. Bopp, M. Gehlen, B. Schneider, P. Cadule, T. L. Frölicher, J. Segschneider, J. Tjiputra, C. Heinze, and F. Joos (2011), Regional impacts of climate change and atmospheric CO_2 on future ocean carbon uptake: A multimodel linear feedback analysis, *J. Clim.*, *24*(9), 2300–2318, doi:10.1175/2010JCLI3787.1.

Sarmiento, J. L., and N. Gruber (2006), *Ocean Biogeochemical Dynamics*, Princeton Univ. Press, Princeton, N. J.

Siegel, D. A., et al. (2016), Prediction of the export and fate of global ocean net primary production: The EXPORTS science plan, *Front. Mar. Sci.*, *3*(22), doi:10.3389/fmars.2016.00022.

Takahashi, T., J. Olafsson, J. G. Goddard, D. W. Chipman, and S. C. Sutherland (1993), Seasonal variation of CO_2 and nutrients in the high-latitude surface oceans: A comparative study, *Global Biogeochem. Cycles*, *7*(4), 843–878.

Takahashi, T., et al. (2002), Global sea-air CO_2 flux based on climatological surface ocean pCO_2, and seasonal biological and temperature effects, *Deep Sea Res., Part II*, *49*, 1601–1622.

Takahashi, T., et al. (2009), Climatological mean and decadal change in surface ocean pCO_2, and net sea-air CO_2 flux over the global oceans, *Deep Sea Res., Part II*, *56*, 554–577, doi:10.1016/j.dsr2.2008.12.009.

van Heuven, S., D. Pierrot, E. L. J.W.B. Rae, and D. W. R. Wallace (2011), MATLAB program developed for CO_2 system calculations, doi:10.3334/CDIAC/otg.CO2SYS_MATLAB_v1.1.

Wanninkhof, R. (1992), Relationship between wind speed and gas exchange over the ocean, *J. Geophys. Res.*, *97*(C5), 7373–7382, doi:10.1029/92JC00188.

Wanninkhof, R., et al. (2013), Global ocean carbon uptake: Magnitude, variability and trends, *Biogeosciences*, *10*(3), 1983–2000, doi:10.5194/bg-10-1983-2013.

Weiss, R. (1974), Carbon dioxide in water and seawater: The solubility of a non-ideal gas, *Mar. Chem.*, *2*(3), 203–215.

Wong, C. S., N. A. D. Waser, Y. Nojiri, F. A. Whitney, J. S. Page, and J. Zeng (2002), Seasonal cycles of nutrients and dissolved inorganic carbon at high and mid latitudes in the North Pacific Ocean during the Skaugran cruises: Determination of new production and nutrient uptake ratios, *Deep Sea Res., Part II*, *49*, 5317–5338.